Journal of Non-Crystalline Solids 618 (2023) 122516

Contents lists available at ScienceDirect

Journal of Non-Crystalline Solids

journal homepage: www.elsevier.com/locate/jnoncrysol

Pressure-induced reversible structural phase transitions and metallization in GeTe under hydrostatic and non-hydrostatic environments up to 22.9 GPa

Xinyu Zhang [a,b], Lidong Dai [a,*], Haiying Hu [a,*], Meiling Hong [a], Chuang Li [a,b]

[a] Key Laboratory of High-temperature and High-pressure Study of the Earth's Interior, Institute of Geochemistry, Chinese Academy of Sciences, Guiyang, Guizhou 550081, China
[b] University of Chinese Academy of Sciences, Beijing 100049, China

ARTICLE INFO

Keywords:
GeTe
Raman spectroscopy
Electrical conductivity
Phase transition
Metallization
High pressure

ABSTRACT

The pressure-dependent vibrational and electrical transport properties of GeTe have been investigated in a diamond anvil cell through *in-situ* Raman spectroscopy and electrical conductivity measurements under hydrostatic and non-hydrostatic environments up to 22.9 GPa. Upon compression, two structural transformations from rhombohedral to cubic NaCl-type to orthorhombic GeTe occurred at 3.2 GPa and 12.3 GPa under non-hydrostatic condition. Similarly, two corresponding phase transitions were detected at much higher pressures of 5.0 GPa and 15.4 GPa under hydrostatic condition. Additionally, a 3.3 GPa of electronic transition accompanying by the rhombohedral to cubic NaCl-type transition was characterized by the variable-temperature electrical conductivity experiments. Upon decompression, the recoverable Raman spectra and resumable electrical conductivity suggested that the structural and electronic transitions of GeTe were reversible. The reversibility was further confirmed by the microscopic structural observations from high-resolution transmission electron microscopy, fast Fourier transform and atomic force microscopy.

1. Introduction

In the recent decades, binary IV-VI germanium monochalcogenides GeX (X = S, Se and Te) have raised considerable attention because of their extraordinary and novel physical and chemical properties, which is widely used in optoelectronic applications and data-storage devices [1–8]. As a representative semiconductor of GeX family, layered GeTe is of great potential and interest in the field of phase change random access memory (PCRAM) due to its unique transformation between its amorphous state and crystal state [9–11]. At ambient conditions, different from GeS and GeSe with orthorhombic structure, crystalline GeTe adopts a rhombohedral structure (a distorted NaCl-type structure) with a narrow band gap energy of 0.23 eV [12].

In general, the application of pressure can induce some dramatic changes for IV-VI semiconductors in their crystal and electronic structures away from the pristine state, leading to the appearance of high-pressure polymorphs. A significant number of experimental investigations on the high-pressure phase stability and structural transitions of GeTe have been performed by virtue of X-ray diffraction, electrical resistance measurements and Raman spectroscopy [13–16]. All of these previously available results showed that the rhombohedral GeTe firstly transforms into a cubic NaCl-type structure and then into an orthorhombic structure with increasing pressure. However, there exists considerable controversy concerning the high-pressure phase transition pressures. Leger and Redon [13] investigated the phase transformation of GeTe up to 25.0 GPa by powder X-ray diffraction experiments using a solid pressure medium of silicone grease and they found two pressure-induced phase transitions from the rhombohedral to cubic NaCl-type to orthorhombic structures at the respective pressures of 4.0 GPa and 12.0 GPa. Whereas, a higher transition pressure of 19.2 GPa of the cubic NaCl-type to orthorhombic phases was reported by Serebryanaya et al. [14] through X-ray diffraction study under share deformation. Subsequently, Onodera et al. [15] conducted the electrical resistance measurements of GeTe in conjunction with X-ray diffraction experiments to investigate its high-pressure electrical and structural properties with the pressure medium of a mixture of methanol, ethanol and water (volume ratio of 16:3:1). Their results revealed the rhombohedral to cubic NaCl-type structural transition at 3.0 GPa and the cubic

* Corresponding authors.
E-mail addresses: dailidong@vip.gyig.ac.cn (L. Dai), huhaiying@vip.gyig.ac.cn (H. Hu).

https://doi.org/10.1016/j.jnoncrysol.2023.122516
Received 22 April 2023; Received in revised form 17 July 2023; Accepted 20 July 2023
Available online 25 July 2023

NaCl-type to orthorhombic phase transformation at 18.0 GPa. Recently, Pawbake et al. [16] further explored the high-pressure phase transitions of GeTe by a combination of Raman scattering experiments using the pressure medium of neon and first-principles theoretical calculations up to 57.0 GPa. They also identified two pressure-induced phase transitions in GeTe: the rhombohedral-to-cubic transition at 4.0 GPa and the cubic-to-orthorhombic transition at 15.0 GPa. In comprehensive consideration of these previously available results, the hydrostaticity in the sample cell could be one of the crucial influence factors for the discrepancy in the phase transition pressures of GeTe. Moreover, in our previous work, structural transition pressures of the layered metallic chalcogenides (e.g., ZnSe, HfS_2, SnS_2, ReS_2, MoS_2, $MoSe_2$, $MoTe_2$, Ga_2S_3, Ga_2Se_3, As_2Te_3) have been found to be highly sensitive to the hydrostaticity within the sample chamber [17–26]. Consequently, it is vital to systematically investigate the phase stability and structural transitions of GeTe under hydrostatic and non-hydrostatic environments.

On the other hand, there exists large discrepancy on the semiconductor-to-metal phase transition pressure of GeTe between experiments and theoretical calculations [27–31]. Experimentally, Narozhnyi et al. [29] and Wang et al. [31] reported that the metallization of GeTe occurred at the pressure points of 44.0 GPa and 11.0 GPa, respectively. Furthermore, a great number of theoretical calculations on GeTe have been performed to explore its electronic transition at high pressure and these results suggested that the rhombohedral GeTe will undergo a semiconducting to metallic transformation at 5–6 GPa [27,28,30].

In the present studies, we investigated the high-pressure phase transitions and metallization of GeTe under hydrostatic and non-hydrostatic environments up to 22.9 GPa in a diamond cell using *in-situ* Raman spectroscopy, electrical conductivity measurements, high-resolution transmission electron microscopy (HRTEM) and atomic force microscopy (AFM). Our Raman scattering and electrical conductivity results revealed two pressure-induced phase transitions of GeTe from rhombohedral to cubic NaCl-type to orthorhombic structures at the respective pressures of 3.2 GPa and 12.3 GPa under non-hydrostatic condition. As for the hydrostatic condition, two corresponding higher phase transition pressures of 5.0 GPa and 15.4 GPa were detected, respectively. Furthermore, a pressure-induced semiconductor-to-metal transition in GeTe was confirmed at the pressure of 3.3 GPa, which was evidenced by a series of variable-temperature electrical conductivity measurements. The reversible behavior in sample was clearly demonstrated by a series of microscopic observations including the HRTEM, fast Fourier transform (FFT) and AFM. In addition, the influence of the hydrostaticity under hydrostatic and non-hydrostatic environments on the phase transition pressures of GeTe were detailedly discussed.

2. Materials and methods

2.1. Sample preparation and characterization

Germanium telluride (GeTe) with high purity (99.99%) was commercially purchased from Hangzhou Kaiyada Company (Hangzhou city, Zhejiang province, China). The experimental sample was characterized by X-ray diffraction (XRD) experiments using a PIXcel3D area detector under the conditions of X-ray wavelength: 1.5406 Å, working voltage: 2.2 kV and resolution: 0.028° over a larger 2θ range from 10° to 70° at the State Key Laboratory of Ore Deposit Geochemistry, Institute of Geochemistry, Chinese Academy of Sciences. As displayed in Fig. 1(a), our collected X-ray diffraction pattern of GeTe at ambient conditions can be well indexed into a rhombohedral structure (space group: *R3m*) with the following lattice parameters obtained by the Rietveld refinement with R_{wp} factor of 5.76% using the general structure analysis system (GSAS) with EXPGUI software [32]: $a = b = 8.339 \pm 0.002$ Å, $c = 10.662 \pm 0.003$ Å, $\alpha = \beta = 90°$, $\gamma = 120°$ and $V = 642.07 \pm 0.49$ Å^3 (JCPDS No.47–1079), which is in good agreement with the previous results on crystalline GeTe [33,34]. Fig. 1(b) presents the energy-dispersive X-ray spectroscopy (EDXS) of sample. The strong Ge and Te peaks demonstrate that the sample used in the present experiments are pure GeTe. Quantitative composition analysis showed that the atomic percentage of Ge and Te atoms are 48.50% and 51.49%, respectively, and that the chemical composition is $Ge_{0.94}Te$ with the 6 percentages of germanium atomic vacancy, indicating a high quality of the starting sample used in our present high-pressure experiments.

2.2. High-pressure raman measurements

High-pressure Raman scattering experiments of GeTe were carried out using a piston-cylinder diamond anvil cell (DAC) with a 300-μm anvil culet. A piece of T-301 stainless steel gasket with a three-dimensional size of 5 mm × 5 mm × 0.25 mm was pre-indented to 50-μm thickness. In the center of the pre-indented area, a 120-μm sample chamber was prepared utilizing a laser drilling machine. Afterwards, experimental samples and some tiny ruby spheres were loaded into the sample chamber. Pressure in the cell was calibrated in the light of the wavenumber shift of the Cr^{3+} fluorescence peak of ruby [35]. Helium was employed as the pressure-transmitting medium to reach a hydrostatic condition and no pressure medium was used to meet a non-hydrostatic condition. The uncertainties of pressure determination under non-hydrostatic and hydrostatic environments were smaller than 6% and 3%, respectively. High-pressure Raman scattering measurements of GeTe were performed using a confocal Raman spectrometer (Invia, Renishaw 2000, England) and an Olympus charge-coupled device camera under the low laser power of 1 mW to avoid the undesired heat effect due to the laser absorption of sample. The Raman spectra

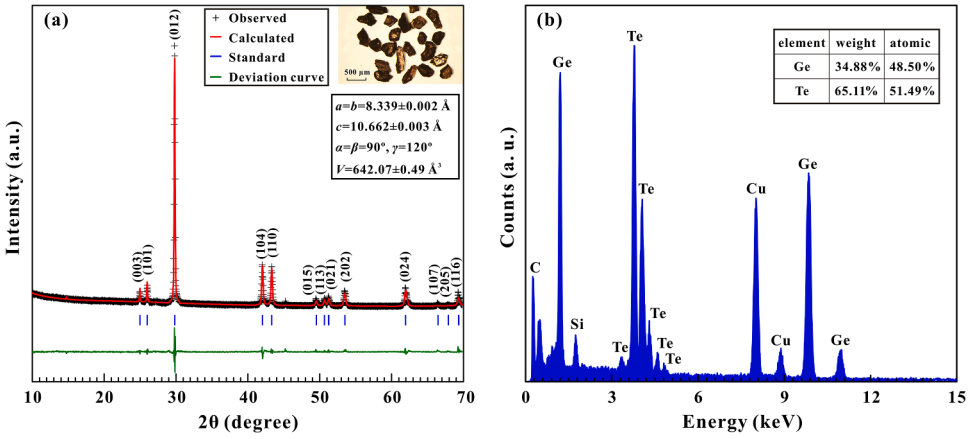

Fig. 1. (a) The X-ray diffraction pattern and Rietveld refinement results of GeTe at ambient conditions. Inset: the image of the starting GeTe sample. The red solid line is the calculated data and the black cross symbols are the observed data. The vertical blue bars represent the standard positions of the Bragg peaks. The deviation curve between observed and calculated patterns is placed at the bottom. (b) EDXS image of crystalline GeTe. Some carbon– and silicon–containing film basements are also observed in these of representative characteristic patterns.

were collected in the wavenumber range of 100–250 cm^{-1} with the spectral precision of 1 cm^{-1} in the backscattering geometry. The acquisition time for each Raman spectrum was set as 180 s. In order to avoid undulating pressure, a ten-minute interval was controlled between Raman measurements at each pre-designed pressure.

2.3. High-pressure electrical conductivity measurements

High-pressure electrical conductivity experiments of GeTe were conducted using a four-column type DAC with a couple of symmetrical 300-μm anvil culets, which has been extensively used in our previous electrical conductivity measurements [36–38]. Insulating sample chamber was prepared by compressing a mixture of cubic boron nitride (c-BN) and epoxy resin powders into a pre-indented T-301 gasket with a 240-μm central hole. Subsequently, a new central hole with a 150-μm diameter was laser-drilled. Platinum electrodes were integrated separately onto the diamond anvils. No pressure medium was used in order to prevent additional impurity and to guarantee a good contact between the sample and electrodes. In the high-pressure electrical conductivity measurements, the pressure was calibrated by the high-frequency edge of the first-order Raman spectra of diamond anvils up to 9.5 GPa in order to avoid the influence of ruby on the electrical conductivity of GeTe sample, which shows a high accuracy less than 5% [39,40]. The alternating current (AC) impedance spectra of GeTe were measured utilizing the Solartron-1260 impedance/gain phase analyzer within a frequency range from 0.1 Hz to 10^7 Hz at a preset signal voltage of 3.0 V. For the high-pressure variable-temperature electrical conductivity measurements, low temperature was attained by the volatilization of liquid nitrogen. The variation of experimental temperature was monitored through a *k*-type thermocouple attached to the side of a diamond. The detailed descriptions on the high-pressure experimental methods and measurement procedures can be found in our published work [17,36,37].

3. Results and discussion

3.1. High-pressure Raman spectroscopy measurements

The *in-situ* vibrational properties of GeTe have been systematically investigated under hydrostatic and non-hydrostatic environments at pressures up to 22.9 GPa. As displayed in Fig. 2(a), at the pressure of 0.6 GPa, two prominent Raman-active peaks can be clearly observed in the wavenumber range of 100–250 cm^{-1}. According to previously available Raman scattering results on GeTe [16,41], the Raman characteristic peak at 124 cm^{-1} can be assigned as the A_1 symmetry transverse optical mode. The Raman peak at the position of 140 cm^{-1} (defined as M_1) is related to an important bulk lattice vibration of GeTe [42].

Under non-hydrostatic condition, Fig. 2(a) exhibits the Raman spectra of GeTe with increasing pressure up to 22.9 GPa upon compression and the subsequent Raman spectrum upon decompression to atmospheric pressure. Fig. 2(b) displays the corresponding Raman shifts of GeTe as a function of pressure. From Fig. 2, we can unambiguously identify three discrete segments on the base of the evolutions of the pressure-dependent Raman spectra and Raman shifts: (i) within the pressure range of 0.6–2.7 GPa, the A_1 mode tended to monotonously shift towards lower wavenumber range with a larger negative $d\omega/dP$ value (ω represents Raman shift and P is pressure) of –5.01 cm^{-1} GPa^{-1} and exhibited an obvious red shift behavior. The M_1 mode seemed to be a weak relationship of pressure with a tiny $d\omega/dP$ value of 0.04 cm^{-1} GPa^{-1}. It should be noted that, in this pressure range, the A_1 mode displayed prominent phonon softening with the rise of pressure, which indicates the structural instability of sample [16,43]; (ii) at the middle pressure range of 3.2–11.5 GPa, the A_1 and M_1 modes lost their peaks and two extremely weak and broad humps at around 110 cm^{-1} and 150 cm^{-1} were observed; (iii) in the higher pressure range of 12.3–22.9 GPa, two absolutely new Raman peaks located at 164 cm^{-1} and 182 cm^{-1} (defined as M_2 and M_3 modes, respectively) emerged and both of them showed obvious blue shifts with high $d\omega/dP$ values of 2.33 cm^{-1} GPa^{-1}

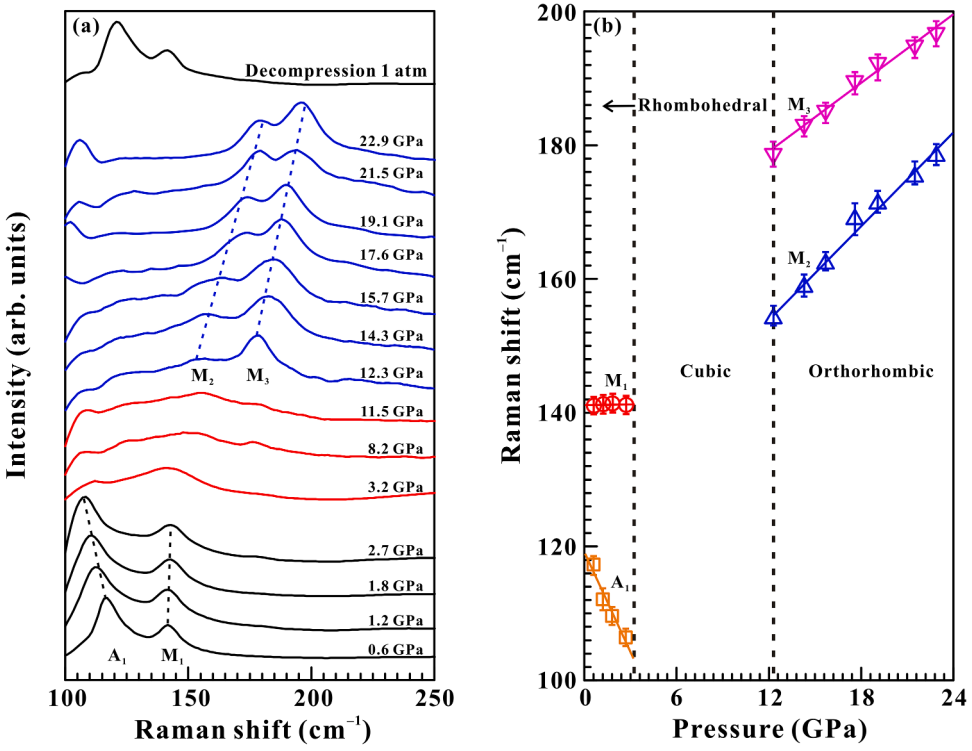

Fig. 2. Raman spectroscopic results of GeTe at different pressure points under non-hydrostatic condition. (a) Raman spectra of GeTe at some representative high-pressure points up to 22.9 GPa. (b) The pressure dependence of the Raman shifts of A_1, M_1, M_2 and M_3 modes for GeTe. The colored solid and dashed lines are used to guide to the eyes.

and 1.71 cm^{-1} GPa^{-1}, respectively. In sum, the softening of A_1 mode and the disappearance of A_1 and M_1 modes at 3.2 GPa provided probable spectroscopic clues to support a pressure-induced structural phase transition from rhombohedral GeTe to cubic NaCl-type GeTe [16,44]. With increasing pressure up to 12.3 GPa, the emergence of the absolutely new Raman peaks of M_2 and M_3 also offered a possible evidence for another phase transition in GeTe, which has been attributed to the cubic NaCl-type to orthorhombic phase transition in the light of high-pressure X-ray diffraction experimental results by Leger and Redon [13] and Serebryanaya et al. [14]. Upon decompression to atmospheric pressure, the collected Raman spectrum was identical to that of the starting GeTe sample, indicating that the phase transition of GeTe is reversible under non-hydrostatic condition.

Under hydrostatic condition, the relationship of the Raman spectra and Raman shifts of GeTe with increasing pressure up to 22.7 GPa is displayed in Fig. 3. It is obvious that the disappearance of the A_1 and M_1 modes and the occurrence of the M_2 and M_3 modes took place at higher pressure points of 5.0 GPa and 15.4 GPa, respectively, which may be strongly correlated with the phase transformations from the rhombohedral to cubic NaCl-type to orthorhombic structures in GeTe. After releasing to atmospheric pressure, the recoverable Raman spectrum hints reversible phase transition of GeTe under hydrostatic condition. In addition, Table 1 summarizes the detailed $d\omega/dP$ values of the Raman modes of A_1, M_1, M_2 and M_3 under hydrostatic and non-hydrostatic environments. It can be clearly seen from Table 1 that, under both non-hydrostatic and hydrostatic environments, the A_1 modes showed stronger pressure dependence with the respective $d\omega/dP$ values of –5.01 cm^{-1} GPa^{-1} and –2.51 cm^{-1} GPa^{-1}, whereas the M_1 modes exhibited a plateau with feeble $d\omega/dP$ values of 0.04 cm^{-1} GPa^{-1} and 0.06 cm^{-1} GPa^{-1}. Under higher pressure conditions, for the M_2 and M_3 modes, their pressure coefficients under non-hydrostatic condition, which were fitted as 2.33 cm^{-1} GPa^{-1} and 1.71 cm^{-1} GPa^{-1}, respectively, are smaller than those under non-hydrostatic condition (3.05 cm^{-1} GPa^{-1} and 2.29 cm^{-1} GPa^{-1}). According to the present Raman results obtained from hydrostatic and non-hydrostatic environments, it is quite clear that the non-hydrostatic condition lowered the transition pressure from 5.0 GPa to 3.2 GPa for the rhombohedral-to-cubic transition and from 15.4 GPa to 12.3 GPa for the cubic-to-orthorhombic transition in GeTe. A possible reason for the decrease of the transition pressures in non-hydrostatic condition is due to the influence of deviatoric stresses [45]. Larger deviatoric stresses were generated under non-hydrostatic condition, which will decrease the pressure points of structural phase transitions in layered GeTe. As a matter of fact, similar phenomena have been already revealed in our previous work among other layered metallic chalcogenides (e.g., ZnSe, HfS_2, SnS_2, ReS_2, MoS_2, $MoSe_2$, $MoTe_2$, Ga_2Se_3, As_2Te_3) [17–22,24–26].

Table 1
Pressure dependence of the Raman shifts for GeTe under non-hydrostatic and hydrostatic environments. ω: Raman shift; P: pressure.

Pressure conditions	Pressure ranges	A_1	M_1	M_2	M_3
Non-hydrostatic	0.6 GPa < $d\omega/dP$ < 2.7 GPa	–5.01 (21)	0.04 (1)	—	—
	3.2 GPa < $d\omega/dP$ < 11.5 GPa	—	—	—	—
	12.3 GPa < $d\omega/dP$ < 22.9 GPa	—	—	2.33 (12)	1.71 (9)
Hydrostatic	0.4 GPa < $d\omega/dP$ < 4.5 GPa	–2.51 (15)	0.06 (1)	—	—
	5.0 GPa < $d\omega/dP$ < 14.5 GPa	—	—	—	—
	15.4 GPa < $d\omega/dP$ < 22.7 GPa	—	—	3.05 (16)	2.29 (13)

3.2. High-pressure electrical conductivity measurements

The *in-situ* electrical conductivity experiments of GeTe at high pressures up to 9.5 GPa were conducted through AC impedance

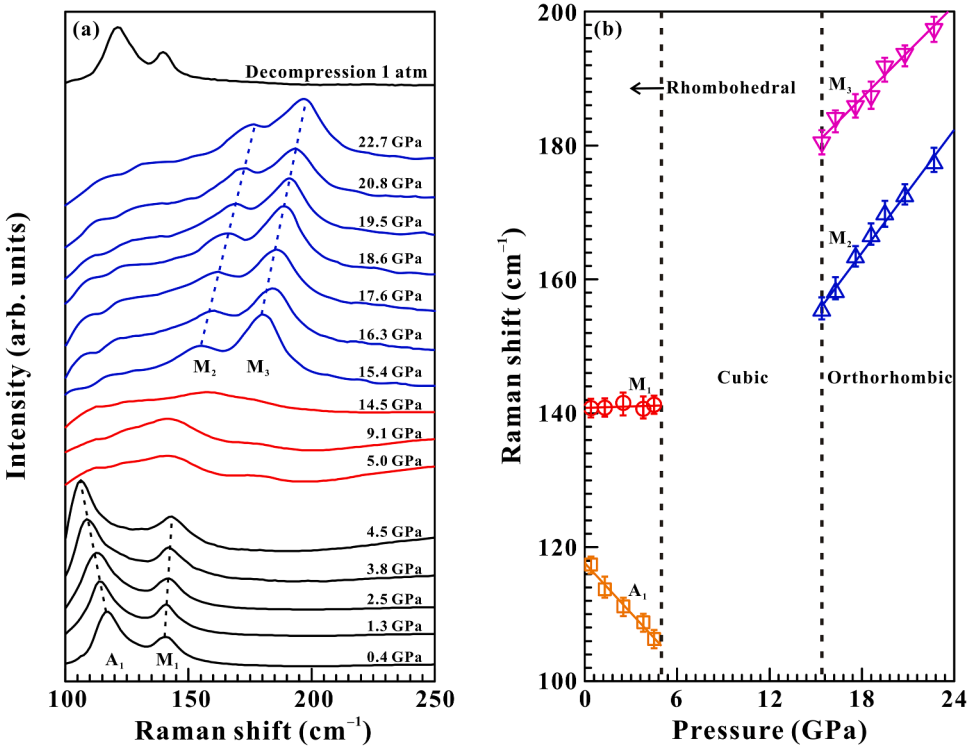

Fig. 3. Raman spectroscopic results of GeTe at different pressure points under hydrostatic condition. (a) Raman spectra of GeTe at some representative high-pressure points up to 22.7 GPa. (b) The pressure dependence of the Raman shifts of A_1, M_1, M_2 and M_3 modes for GeTe. The colored solid and dashed lines are used to guide to the eyes.

spectroscopy method to explore its electrical transport property. Fig. 4 (a) exhibits the measured Nyquist plots including a semicircular arc at the high frequencies (~10^3–10^7 Hz) on the left and an oblique line at the low frequencies (10^{-1}–~10^3 Hz) on the right at the pressure range of 0.5–2.4 GPa, which are representative of the grain interior resistance and the grain boundary resistance for sample, respectively. Figs. 4(b) and 4(c) show the impedance spectra with an oblique line way in the fourth quadrant at pressures from 3.0 GPa to 9.5 GPa. All of these collected impedance spectroscopy results were fitted utilizing the ZView software by an equivalent circuit consisting of two series sections (Each section is composed of one resistance (R) and one constant phase element (CPE) in parallel) for Fig. 4(a) and by one resistance (R) for Fig. 4(b) and (c). The measurement errors from the data fitting of impedance spectra were controlled less than 5%.

The electrical conductivity of sample (σ) is calculated by the equation: $\sigma = L/SR$, where L is the experimental sample length (cm), S is the cross-section area of the electrode (cm^2) and R is the resistance of the sample (R). In the present work, Fig. 4(d) shows the pressure dependence of the logarithmic electrical conductivity of GeTe in the both processes of compression and decompression, and makes it clear that two obviously different pressure ranges (i.e., 0.5–3.0 GPa and 3.0–9.5 GPa) can be distinguished from the discontinuity in the pressure-dependent logarithmic electrical conductivity. More specifically, in the pressure range of 0.5–3.0 GPa, the electrical conductivity dramatically increased by near four orders of magnitude with a steep slope of 1.61 S cm^{-1} GPa^{-1}. When pressure was further increased from 3.0 GPa to 9.5 GPa, a feeble change in the logarithmic electrical conductivity from 0.54 S cm^{-1} to 0.72 S cm^{-1} with a tiny slope of 0.02 S cm^{-1} GPa^{-1} was acquired. Thus, the striking discontinuity in the pressure-dependent logarithmic electrical conductivity was observable at the pressure of 3.0 GPa, which is probably related to the phase transition from the rhombohedral to cubic NaCl-type GeTe as observed in the above-mentioned Raman scattering results under non-hydrostatic condition. Furthermore, these relatively high logarithmic electrical conductivity values of 0.54–0.72 S cm^{-1} beyond 3.0 GPa is typically metallic characteristics, and thus, it is reasonable to extrapolate that the phase transition at 3.0 GPa is possibly related to a semiconductor-to-metal transformation in GeTe. During the process of decompression, the logarithmic electrical conductivity of sample reduced gradually from 0.72 S cm^{-1} to –2.79 S cm^{-1} when pressure was released from 9.1 GPa to 0.6 GPa, suggesting that the electronic transition is reversible. It is also worth noting that there is a hysteresis effect in the pressure-dependent logarithmic electrical conductivity upon decompression compared with compression process for the semiconductor-to-metal phase transition. This could be related to the creation of defects during the successive phase transitions as shown in the related compound InSe when it undergoes the rhombohedral-to-cubic phase transition [46].

In order to further explore the metallic behavior of GeTe under high pressures, variable-temperature electrical conductivity measurements were performed in the temperature range of 120–300 K. Fig. 5(a) displays the *in-situ* temperature-dependent logarithmic electrical conductivity of GeTe at five representative pressure points of 0.8, 2.2, 3.3, 6.8, and 9.1 GPa. Three unapparent trend lines at 3.3, 6.8 and 9.1 GPa were magnified in Fig. 5(b)–5(d), respectively, to clearly observe the variation trends of the electrical conductivity with the increasing temperature. In general, semiconductors are characterized by a positive

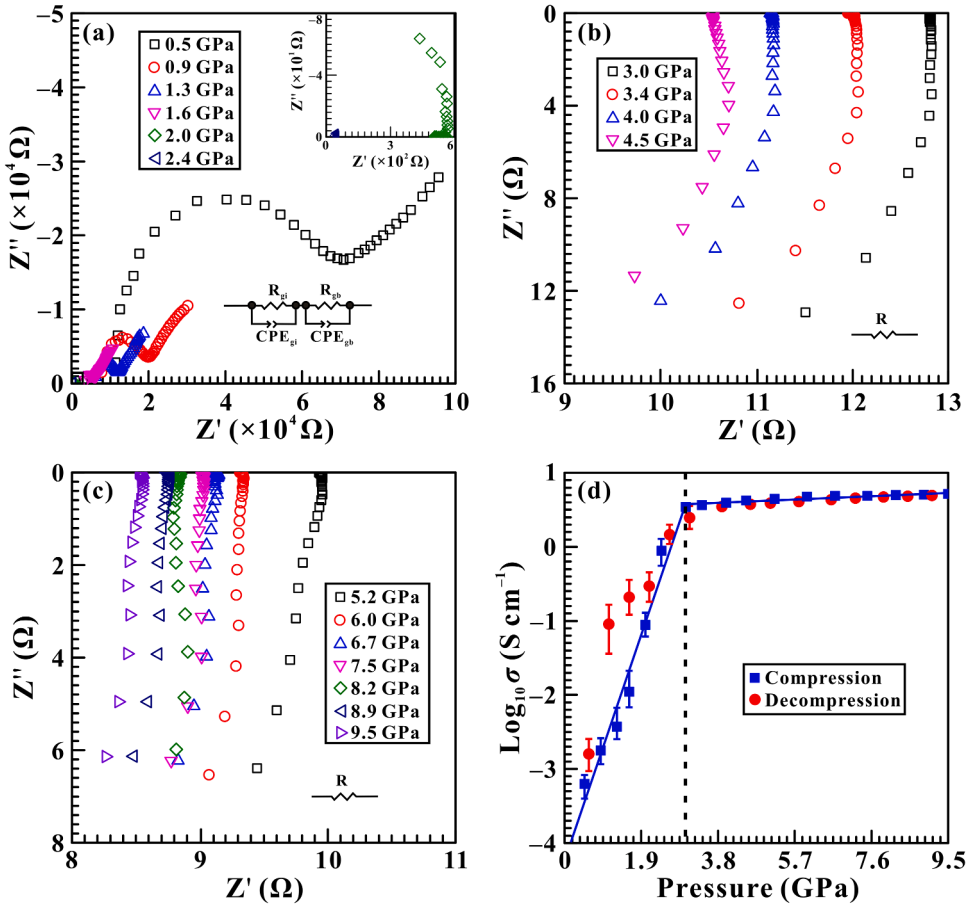

Fig. 4. Complex impedance spectra of GeTe under pressures up to 9.5 GPa. (a) 0.5–2.4 GPa. (b) 3.0–4.5 GPa. (c) 5.2–9.5 GPa. (d) The pressure dependence of the logarithmic electrical conductivity of GeTe in the both processes of compression and decompression. The blue solid line and the black dashed line are used to guide to the eyes.

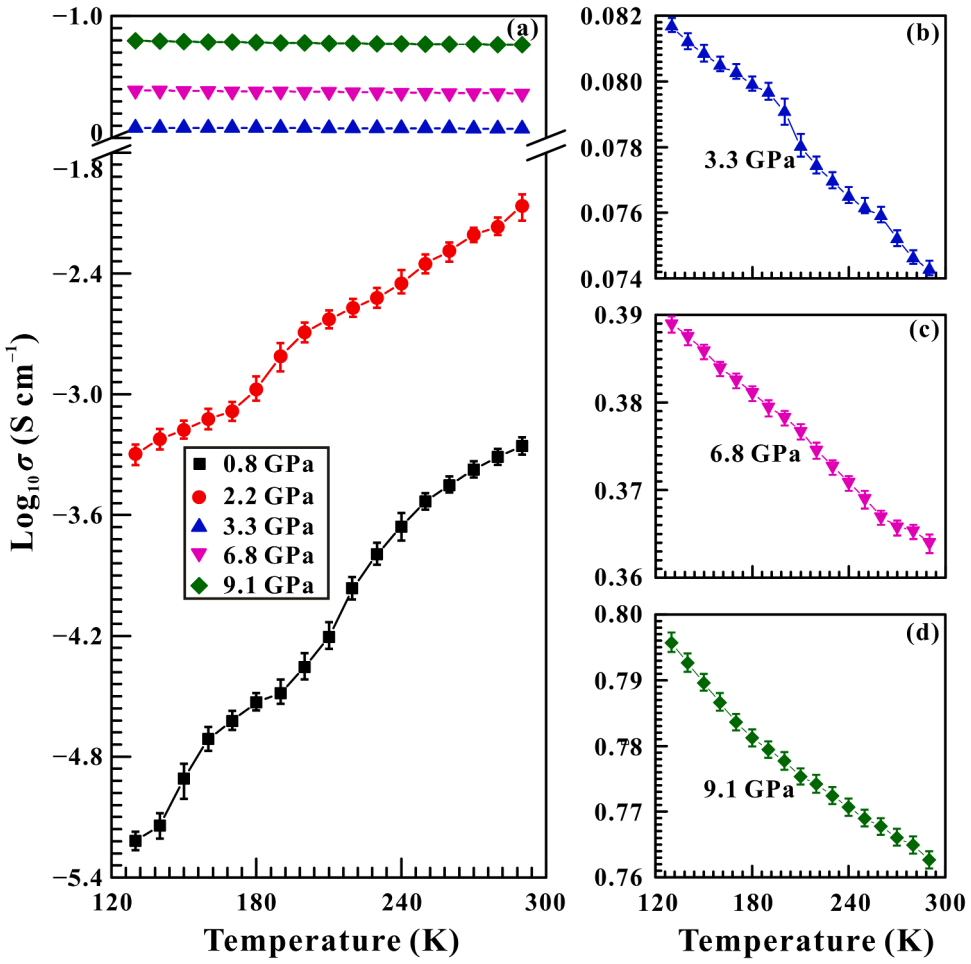

Fig. 5. The temperature-dependent logarithmic electrical conductivity of GeTe at certain representative pressure points in the temperature range of 120–300 K. (a) Pressures are at 0.8, 2.2, 3.3, 6.8 and 9.1 GPa. (b), (c) and (d) The magnified figures of three trend lines for the logarithmic electrical conductivity with temperature at pressures of 3.3, 6.8 and 9.1 GPa, respectively.

temperature dependence of electrical conductivity, whereas a negative temperature-dependent electrical conductivity curve can be observed in metals [23,36,47,48]. In the relatively lower pressure range from 0.8 GPa to 2.2 GPa, the monotonic enhancement in the logarithmic electrical conductivity with increasing temperature clearly disclosed the semiconducting behavior of GeTe. In contrast, the logarithmic electrical conductivity at 3.3, 6.8 and 9.1 GPa are of a negative relation with the increase of temperature, implying the metallic property of sample. In here, a series of temperature-dependent electrical conductivity results indicated that the metallization emerges at 3.3 GPa, which is very close to the rhombohedral to cubic NaCl-type phase transition of GeTe. Although in comparison with the previous investigations on the metallization of GeTe by Narozhnyi et al. [29] and Wang et al. [31], a deviation in the metallization pressure was obtained, which may originate from the different experimental method, pressure calibration and pressure-transmitting medium, our acquired metallization pressure is in good agreement with the results from theoretical calculations [27,28,30]. Similarly, the pressure-induced metallized phenomena have also been observed in other germanium-bearing monochalcogenides of GeSe and GeS, as listed in Table 2 [15,27–31,49–51]. In addition, Table 3 lists the phase transition pressures of GeTe from rhombohedral to cubic NaCl-type to orthorhombic structures using helium and no pressure medium in the present investigations in comparison with different pressure-transmitting mediums including a mixture of methanol, ethanol and water, silicone grease and neon in previous high-pressure studies. From Table 3, it seems that the more rigid the pressure-transmitting mediums are, the smaller the phase transition pressures become. In the present results, the lower phase transition pressures of 3.2 GPa and 12.3 GPa were obtained for the rhombohedral to cubic NaCl-type phase transition and the cubic NaCl-type to orthorhombic phase transition in GeTe under non-hydrostatic condition using no pressure-transmitting medium, which are comparable to the phase transition pressures of 4.0 GPa and 12.0 GPa using silicone grease as pressure-transmitting medium [13]. Under hydrostatic condition of gaseous helium, higher transition pressures of 5.0 GPa and 15.4 GPa were observed, in good agreement with the results of 4.0 GPa and 15.0 GPa with the pressure-transmitting medium of gaseous neon [16]. In the

Table 2
Comparison of the pressure points of metallic phase transition for GeTe with two representative germanium monochalcogenides (i.e., GeS and GeSe) in previous experimental and theoretical investigations. In here, P_m stands for the pressure point of metallization.

Germanium monochalcogenides	P_m (GPa)	References
GeTe	3.3	This study
	5.0	[30]
	5.4	[27]
	6.0	[28]
	11.0	[31]
	44.0	[29]
GeSe	6.0	[49]
	25.0	[15]
	25.0	[50]
GeS	20.0	[51]

Table 3
Comparison of phase transition pressures in GeTe under non-hydrostatic and hydrostatic environments with the previously reported results.

High-pressure experiments	Pressure-transmitting mediums	P_{t1} (GPa)	P_{t2} (GPa)	References
Raman	No pressure medium	3.2	12.3	This study
Raman	Helium	5.0	15.4	This study
X-ray diffraction	Silicone grease	4.0	12.0	[13]
X-ray diffraction	Methanol, ethanol and water	3.0	18.0	[15]
Raman	Neon	4.0	15.0	[16]

Note: P_{t1} represents the phase transition pressure from rhombohedral to cubic NaCl-type structures. P_{t2} represents the phase transition pressure from cubic NaCl-type to orthorhombic structures.

pressure-transmitting medium of a mixture of methanol, ethanol and water (volume ratio of 16:3:1), a minimum pressure of 3.0 GPa for the rhombohedral-to-cubic transition and a maximum pressure of 18.0 GPa for the cubic-to-orthorhombic transition were obtained by Onodera et al. (1997) [15], which may be due to the uncertainty of calibrating pressure. In worse hydrostaticity such as no pressure-transmitting medium, silicone grease and a mixture of methanol, ethanol and water (volume ratio of 16:3:1), larger deviatoric stresses were generated under high pressures, which will decrease the pressure points of structural phase transitions in layered GeTe in comparison with the gaseous helium and neon which are of good hydrostaticity.

3.3. HRTEM and AFM observations of the starting and recovered samples

In order to explore the microscopical structures and micromorphological variations of the initial sample and the recovered samples under non-hydrostatic and hydrostatic environments, surface microstructural information and morphology observations are obtained by means of HRTEM and AFM. The HRTEM images and their corresponding FFT patterns for the starting and recovered samples are illustrated in Fig. 6. In here, Fig. 6(a)–6(c) are the HRTEM images of the starting sample and the recovered samples decompressed from 21.8 GPa and 22.5 GPa under non-hydrostatic and hydrostatic environments, respectively. Fig. 6(d)–6(f) represent their corresponding FFT patterns. From the HRTEM image of Fig. 6(a), typical lattice fringes were clearly observed with an interplanar spacing of 0.36±0.02 nm for the initial sample, which is well consistent with the (003) crystallographic plane of the rhombohedral GeTe. At the same time, the corresponding FFT pattern with bright and clear diffraction spots (Fig. 6(d)) indicated a highly crystalline structure of the initial sample. Under non-hydrostatic condition, the FFT pattern (Fig. 6(e)) was composed of some different diffraction haloes with many clear and bright spots, which indicates the coexistence of several different crystalline planes. Furthermore, it is obvious from Fig. 6(b) that the corresponding HRTEM image displayed short-range order and various lattice fringes. Under hydrostatic condition, the FFT pattern (Fig. 6(f)) of the recovered sample was consisted of shiny and well-defined diffraction spots, showing the presence of one individual single crystalline plane, and the corresponding HRTEM (Fig. 6(c)) showed a clear long-range order and the uniform crystal plane with the interplanar spacing of 0.34±0.01 nm in the selected area. The faint discrepancy is presumably ascribed to the variation of pressure-transmitting medium under different hydrostatic environments. Under hydrostatic condition, the pressure-transmitting medium of helium would greatly weaken the deviatoric stress in the sample chamber and protect the sample away from damage. Under non-hydrostatic condition, the recovered sample suffered the applied high pressure due to the absence of pressure-transmitting medium, which results in the formation of multi-oriented crystalline planes. In short, our HRTEM and FFT observations implied that the changes in the crystalline structure under hydrostatic and non-hydrostatic environments are reversible upon completely releasing pressure.

Fig. 7 displays the obtained three-dimensional AFM morphology images with a square-area scanning range of 5 μm × 5 μm for the initial

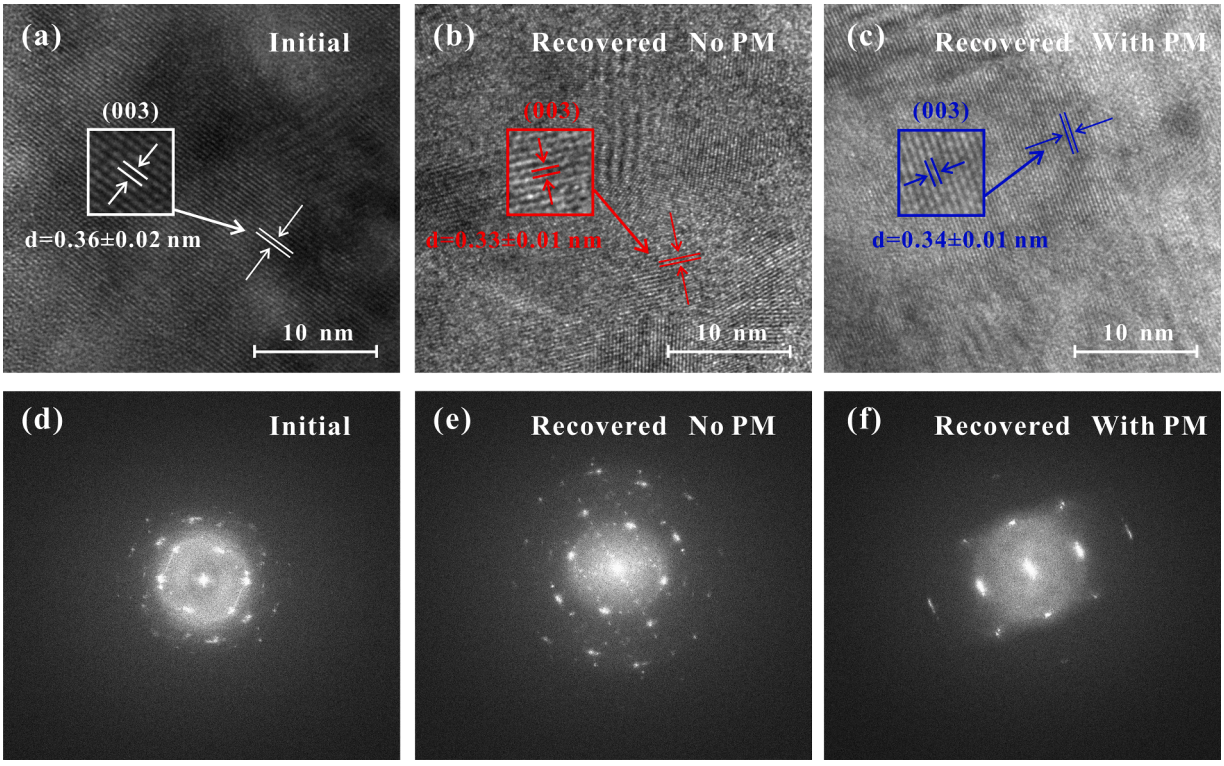

Fig. 6. HRTEM images and FFT patterns of GeTe samples. (a), (b) and (c) are the HRTEM images of the starting sample and the recovered samples decompressed from 21.8 GPa and 22.5 GPa under non-hydrostatic and hydrostatic environments, respectively. (d), (e) and (f) stand for the corresponding FFT patterns of samples. PM: pressure medium.

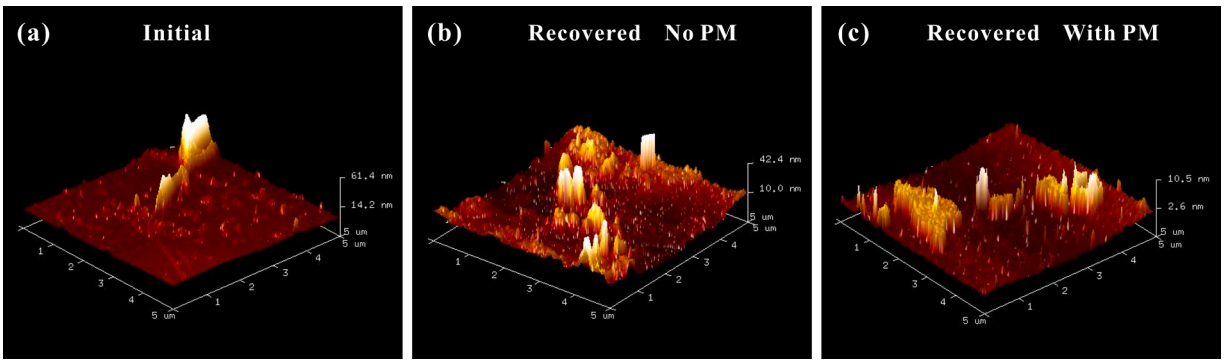

Fig. 7. Three-dimensional AFM morphology images of the GeTe samples with a square-area scanning range of 5 μm × 5 μm. (a) the initial sample. (b) the recovered sample decompressed from 22.1 GPa under non-hydrostatic condition. (c) the recovered sample decompressed from 22.3 GPa under hydrostatic condition. PM: pressure medium.

sample and the recovered GeTe samples decompressed from 22.1 GPa and 22.3 GPa under non-hydrostatic and hydrostatic environments, respectively. All of these AFM images were acquired utilizing a Multimode 8 mass spectrometer (Bruker) by the peak force tapping mode to obtain high-resolution AFM images. As illustrated in Fig. 7, there is no obvious difference in the morphology for the initial and recovered samples. More specifically, all of the initial and recovered samples displayed some easy cleavages in the AFM images, suggesting strong layered features, which is similar to some typically layered metallic chalcogenides (e.g., MoS_2, $MoSe_2$, $MoTe_2$, ReS_2, Sb_2S_3, Ga_2Se_3, As_2Te_3) [16,18,21,22,25,26,36]. A subtle discrepancy from the AFM images is the sample height: ~60 nm for the initial sample; ~40 and ~10 nm for the recovered samples under non-hydrostatic and hydrostatic environments, respectively, which is presumably caused by the reduction of average particle size due to the high pressure. In brief, those microscopic observations from the images of HRTEM, FFT and AFM give solid evidence that the structural phase transition in GeTe is reversible under both non-hydrostatic and hydrostatic environments. This is in good accordance with our high-pressure Raman scattering and electrical conductivity results.

4. Conclusion

In this paper, we reported the reversible high-pressure vibrational and electrical transport behaviors of GeTe under hydrostatic and non-hydrostatic environments up to 22.9 GPa in a DAC using *in-situ* Raman spectroscopy, AC impedance spectroscopy, HRTEM and AFM. Under non-hydrostatic condition, two pressure-induced phase transitions from the rhombohedral to cubic NaCl-type to orthorhombic structures of GeTe occurred at 3.2 GPa and 12.3 GPa, respectively, which were confirmed by the changes of the pressure-dependent Raman peaks and Raman shifts. Under hydrostatic condition, the corresponding phase transitions were revealed at higher pressures of 5.0 GPa and 15.4 GPa, respectively. Furthermore, a semiconductor-to-metal phase transition of GeTe was detected at the pressure of 3.3 GPa, close to the transition to NaCl-type structure. In here, we emphasize the important role of the hydrostaticity within sample chamber, which may be responsible for the discrepancy of the phase transition pressures of GeTe in the present study. Upon decompression, the phase transition of GeTe is reversible as evidenced from the recoverable Raman spectra, electrical conductivity magnitude and the microscopic observations of the HRTEM, FFT and AFM images under both hydrostatic and non-hydrostatic environments.

Author contributions

Lidong Dai and Haiying Hu performed the conceptualization of this article and led the project. Xinyu Zhang, Meiling Hong and Chuang Li performed the investigation including X-ray diffraction (XRD), high-pressure Raman spectra and high-pressure electrical conductivity measurements, high-resolution transmission electron microscopy and atomic force microscopy. Lidong Dai and Xinyu Zhang contributed to the analysis, interpretation and discussion of these results. Xinyu Zhang and Lidong Dai performed the writing-original draft. Lidong Dai, Haiying Hu, Xinyu Zhang, Meiling Hong and Chuang Li performed the writing-review & editing. All the authors commented on the final manuscript. Lidong Dai and Haiying Hu supervised the project.

CRediT authorship contribution statement

Xinyu Zhang: Investigation, Software, Writing – original draft, Writing – review & editing. **Lidong Dai:** Conceptualization, Writing – review & editing. **Haiying Hu:** Conceptualization, Writing – review & editing. **Meiling Hong:** Investigation, Software. **Chuang Li:** Investigation, Software.

Declaration of Competing Interest

The authors declare that they have no known competing financial interests or personal relationships that could have appeared to influence the work reported in this paper.

Data availability

Data will be made available on request.

Acknowledgments

The authors acknowledge the technical support of the *in-situ* high-pressure Raman scattering measurements provided by professor Heping Li at the Key Laboratory of High-temperature and High-pressure Study of the Earth's Interior, Institute of Geochemistry, Chinese Academy of Sciences. This research was financially supported by the National Natural Science Foundation of China (grant number 42072055 and 42274137) and the Youth Innovation Promotion Association of CAS (grant number 2019390).

References

[1] A.L. Greer, N. Mathur, Changing face of the chameleon, Nature 437 (2005) 1246–1247.
[2] H.F. Hamann, M. O'Boyle, Y.C. Martin, M. Rooks, K Wickramasinghe, Ultra-high-density phase-change storage and memory, Nat. Mater. 5 (2006) 383–387.
[3] M.H.R. Lankhorst, B.W.S.M.M. Ketelaars, R.A.M. Wolters, Low-cost and nanoscale non-volatile memory concept for future silicon chips, Nat. Mater. 4 (2005) 347–352.
[4] S. Raoux, W. Welnic, D. Lelmini, Phase change materials and their application to nonvolatile memories, Chem. Rev. 110 (2010) 240–267.

[5] M. Wuttig, Phase-change materials–Towards a universal memory? Nat. Mater. 4 (2005) 265–266.
[6] M. Wuttig, N. Yamada, Phase-change materials for rewriteable data storage, Nat. Mater. 6 (2007) 824–832.
[7] Z.B. Li, Z.Y. Wu, M.J. Feng, X. Wang, W.B. Lu, H.J. Yan, J.S. Hu, D.J. Xue, Crystal stability determination of GeSe allotropes, J. Phys. Chem. C 127 (2023) 10777–10783.
[8] S. Gallego-Parra, E. Bandiello, A. Liang, E. Lora da Silva, P. Rodríguez-Hernández, A. Muñoz, S. Radescu, A.H. Romero, C. Drasar, D. Errandonea, F.J. Manjón, Layered topological semimetal GaGeTe: new polytype with non-centrosymmetric structure, Mater. Today Adv. (2022), 100309, https://doi.org/10.1016/j.mtadv.2022.100309.
[9] J. Akola, R.O. Jones, Structural phase transitions on the nanoscale: the crucial pattern in the phase-change materials $Ge_2Sb_2Te_5$ and GeTe, Phys. Rev. B 76 (2007), 235201, https://doi.org/10.1103/PhysRevB.76.235201.
[10] G. Bruns, P. Merkelbach, C. Schlockermann, M. Salinga, M. Wuttig, T.D. Happ, J. B. Philipp, M. Kund, Nanosecond switching in GeTe phase change memory cells, Appl. Phys. Lett. 95 (2009), 043108, https://doi.org/10.1063/1.3191670.
[11] M. Chen, K.A. Rubin, R.W. Barton, Compound materials for reversible, phase-change optical data storage, Appl. Phys. Lett. 49 (1986) 502–504.
[12] Y.W. Tung, M.L. Cohen, Relativistic band structure and electronic properties of SnTe, GeTe, and PbTe, Phys. Rev. 180 (1969) 823–826.
[13] J.M. Leger, A.M. Redon, Phase transformations and volume of the IV-VI GeTe semiconductor under high pressure, J. Phys.-Condens. Matter. 2 (1990) 5655–5662.
[14] N.R. Serebryanaya, V.D. Blank, V.A. Ivdenko, GeTe-phases under shear deformation and high pressure up to 56 GPa, Phys. Lett. A 197 (1995) 63–66.
[15] A. Onodera, I. Sakamoto, Y. Fujii, N. Môri, S. Sugai, Structural and electrical properties of GeSe and GeTe at high pressure, Phys. Rev. B 56 (1997) 7935–7941.
[16] A. Pawbake, C. Bellin, L. Paulatto, K. Béneut, J. Biscaras, C. Narayana, D.J. Late, A. Shukla, Pressure-induced phase transitions in germanium telluride: raman signatures of anharmonicity and oxidation, Phys. Rev. Lett. 122 (2019), 145701, https://doi.org/10.1103/PhysRevLett.122.145701.
[17] L.D. Dai, Y.K. Zhuang, H.P. Li, L. Wu, H.Y. Hu, K.X. Liu, L.F. Yang, C. Pu, Pressure-induced irreversible amorphization and metallization with a structural phase transition in arsenic telluride, J. Mater. Chem. C 5 (2017) 12157–12162.
[18] M.L. Hong, L.D. Dai, H.Y. Hu, X.Y. Zhang, Pressure-induced structural phase transition and metallization in Ga_2Se_3 up to 40.2 GPa under non-hydrostatic and hydrostatic environments, Crystals 11 (2021) 746, https://doi.org/10.3390/cryst11070746.
[19] M.L. Hong, L.D. Dai, H.Y. Hu, X.Y. Zhang, C. Li, Y. He, High-pressure structural phase transitions and metallization in layered HfS_2 under different hydrostatic environments up to 42.1 GPa, J. Mater. Chem. C 10 (2022) 10541–10550.
[20] C. Pu, L.D. Dai, H.P. Li, H.Y. Hu, K.X. Liu, L.F. Yang, M.L. Hong, Pressure-induced phase transitions of ZnSe under different pressure environments, AIP Adv. 9 (2019), 025004, https://doi.org/10.1063/1.5082209.
[21] L.F. Yang, L.D. Dai, H.P. Li, H.Y. Hu, K.X. Liu, C. Pu, M.L. Hong, P.F. Liu, Pressure-induced metallization in $MoSe_2$ under different pressure conditions, RSC Adv. 9 (2019) 5794–5803.
[22] L.F. Yang, L.D. Dai, H.P. Li, H.Y. Hu, K.X. Liu, C. Pu, M.L. Hong, P.F. Liu, Characterization of the pressure-induced phase transition of metallization for $MoTe_2$ under hydrostatic and non-hydrostatic conditions, AIP Adv 9 (2019), 065104, https://doi.org/10.1063/1.5097428.
[23] L.F. Yang, J.J. Jiang, L.D. Dai, H.Y. Hu, M.L. Hong, X.Y. Zhang, H.P. Li, P.F. Liu, High-pressure structural phase transition and metallization in Ga_2S_3 under non-hydrostatic and hydrostatic conditions up to 36.4 GPa, J. Mater. Chem. C 9 (2021) 2912–2918.
[24] X.Y. Zhang, L.D. Dai, H.Y. Hu, M.L. Hong, C. Li, Pressure-induced coupled structural-electrical transition in SnS_2 under different hydrostatic environments up to 39.7 GPa, RSC Adv. 12 (2022) 2454–2461.
[25] Y.K. Zhuang, L.D. Dai, H.P. Li, H.Y. Hu, K.X. Liu, L.F. Yang, C. Pu, M.L. Hong, P. F. Liu, Deviatoric stresses promoted metallization in rhenium disulfide, J. Phys. D Appl. Phys. 51 (2018), 165101, https://doi.org/10.1088/1361-6463/aab5a7.
[26] Y.K. Zhuang, L.D. Dai, L. Wu, H.P. Li, H.Y. Hu, K.X. Liu, L.F. Yang, C. Pu, Pressure-induced permanent metallization with reversible structural transition in molybdenum disulfide, Appl. Phys. Lett. 110 (2017), 122103, https://doi.org/10.1063/1.4979143.
[27] A. Ciucivara, B.R. Sahu, L. Kleinman, Density functional study of the effect of pressure on the ferroelectric GeTe, Phys. Rev. B 73 (2006), 214105, https://doi.org/10.1103/PhysRevB.73.214105.
[28] G.S. Do, J. Kim, S.H. Jhi, C.H. Park, S.G. Louie, M.L. Cohen, Ab initio calculations of pressure-induced structural phase transitions of GeTe, Phys. Rev. B 82 (2010), 054121, https://doi.org/10.1103/PhysRevB.82.054121.
[29] V.N. Narozhnyi, G.N. Stepanov, E.E. Semenova, Superconductivity of Si, GaP, GeTe at high pressures. Investigation in superconducting anvils, High Press. Res. 10 (1992) 496–499.
[30] Z.M. Sun, J. Zhou, H.K. Mao, R. Ahuja, Peierls distortion mediated reversible phase transition in GeTe under pressure, Proc. Natl. Acad. Sci. U.S.A. 109 (2012) 5948–5952.
[31] Y.Y. Wang, K. Wang, Y.M. Ma, M. Zhou, H.B. Wang, G.T. Liu, Pressure-induced structural transitions between successional superconducting phases in GeTe, J. Phys.: Condens. Matter 33 (2021), 355403, https://doi.org/10.1088/1361-648X/ac0c3a.
[32] A.C. Larson, R.B. Von Dreele, Los Alamos National Laboratory Report LAUR, 2005, pp. 86–748.
[33] T. Chattopadhyay, J.X. Boucherle, H.G. Vonschnering, Neutron diffraction study on the structural phase transition in GeTe, J. Phys. C: Solid State Phys. 20 (1987) 1431–1440.
[34] X.L. Zhou, W.L. Dong, H. Zhang, R.E. Simpson, A zero density change phase change memory material: geTe-O structural characteristics upon crystallization, Sci. Rep. 5 (2015) 11150, https://doi.org/10.1038/srep11150.
[35] H.K. Mao, J. Xu, P.M. Bell, Calibration of the ruby pressure gauge to 800 kbar under quasi-hydrostatic conditions, J. Geophys. Res.: Solid Earth 91 (1986) 4673–4676.
[36] L.D. Dai, K.X. Liu, H.P. Li, L. Wu, H.Y. Hu, Y.K. Zhuang, L.F. Yang, C. Pu, P.F. Liu, Pressure-induced irreversible metallization accompanying the phase transitions in Sb_2S_3, Phys. Rev. B 97 (2018), 024103, https://doi.org/10.1103/PhysRevB.97.024103.
[37] L.D. Dai, C. Pu, H.P. Li, H.Y. Hu, K.X. Liu, L.F. Yang, M.L. Hong, Characterization of metallization and amorphization for GaP under different hydrostatic environments in diamond anvil cell up to 40.0 GPa, Rev. Sci. Instrum. 90 (2019), 066103, https://doi.org/10.1063/1.5093949.
[38] M.L. Hong, L.D. Dai, H.Y. Hu, X.Y. Zhang, C. Li, Y. He, Pressure-induced structural phase transition and metallization of $CrCl_3$ under different hydrostatic environments up to 50.0 GPa, Inorg. Chem. 61 (2022) 4852–4864.
[39] Y. Akahama, H. Kawamura, High-pressure Raman spectroscopy of diamond anvils to 250 GPa: method for pressure determination in the multimegabar pressure range, J. Appl. Phys. 96 (2004) 3748–3751.
[40] Y. Akahama, H. Kawamura, Pressure calibration of diamond anvil Raman gauge to 310 GPa, J. Appl. Phys. 100 (2006), 043516, https://doi.org/10.1063/1.2335683.
[41] U.D. Wdowik, K. Parlinski, S. Rols, T. Chatterji, Soft-phonon mediated structural phase transition in GeTe, Phys. Rev. B 89 (2014), 224306, https://doi.org/10.1103/PhysRevB.89.224306.
[42] K. Jeong, S. Park, D. Park, M. Ahn, J. Han, W. Yang, H.S. Jeong, M.H. Cho, Evolution of crystal structures in GeTe during phase transition, Sci. Rep. 7 (2017) 955, https://doi.org/10.1038/s41598-017-01154-z.
[43] A.K. Liang, S. Rahman, P. Rodriguez-Hernandez, A. Muñoz, F.J. Manjon, G. Nenert, D. Errandonea, High-pressure Raman study of $Fe(IO_3)_3$: soft-mode behavior driven by coordination changes of iodine atoms, J. Phys. Chem. C 124 (2020) 21329–21337.
[44] M.J. Polking, J.J. Urban, D.J. Milliron, H.M. Zheng, E. Chan, M.A. Caldwell, S. Raoux, C.F. Kisielowski, J.W. Ager, R. Ramesh, A.P. Alivisatos, Size-dependent polar ordering in colloidal GeTe nanocrystals, Nano Lett. 11 (2011) 1147–1152.
[45] D. Errandonea, Y. Meng, M. Somayazulu, D. Hausermann, Pressure-induced transition in titanium metal: a systematic study of the effects of uniaxial stress, Physica B: Condens. Matter 355 (2005) 116–125.
[46] F.J. Manjon, D. Errandonea, A. Segura, J.C. Chervin, V. Muñoz, Precursor effects of the rhombohedral-to-cubic phase transition in indium selenide, High Press. Res. 22 (2002) 261–266.
[47] K.X. Liu, L.D. Dai, H.P. Li, H.Y. Hu, L.F. Yang, C. Pu, M.L. Hong, Evidences for phase transition and metallization in β-In_2S_3 at high pressure, Chem. Phys. 524 (2019) 63–69.
[48] A.P. Nayak, S. Bhattacharyya, J. Zhu, J. Liu, X. Wu, T. Pandey, C. Jin, A.K. Singh, D. Akinwande, J.F. Lin, Pressure-induced semiconducting to metallic transition in multilayered molybdenum disulphide, Nat. Commun. 5 (2014) 3731, https://doi.org/10.1038/ncomms4731.
[49] K.L. Bhatia, G. Parthasarathy, D.P. Gosain, E.S.R. Gopal, Pressure-induced first-order transition in layered crystalline semiconductor GeSe to a metallic phase, Phys. Rev. B 33 (1986) 1492–1494.
[50] M. Xu, S. Jakobs, R. Mazzarello, J.Y. Cho, Z. Yang, H. Hollermann, D.S. Shang, X. S. Miao, Z.H. Yu, L. Wang, M. Wuttig, Impact of pressure on the resonant bonding in Chalcogenides, J. Phys. Chem. C 121 (2017) 25447–25454.
[51] R.P. Dias, M. Kim, C.S. Yoo, Structural transitions and metallization in dense GeS, Phys. Rev. B 93 (2016), 104107, https://doi.org/10.1103/PhysRevB.93.104107.